A Kinetic Study of Ovalbumin Fibril Formation

A kinetic study of ovalbumin fibril formation: the importance of fragmentation and end-joining

J. M. D. Kalapothakis[†‡], J. Szavits-Nossan[†], R. J. Morris[†], K. Eden[†], S. Covill[†], S. Tabor[†], J. Gillam[†], P. E. Barran[§], R. J. Allen[†] and C. E. MacPhee[†*]

[†] SUPA, School of Physics and Astronomy, University of Edinburgh, Mayfield Road, Edinburgh EH9 3JZ, United Kingdom; [‡] School of Chemistry, West Mains Road, Edinburgh EH9 3JJ, United Kingdom; [§] School of Chemistry, The University of Manchester, Manchester M13 9PL, United Kingdom

Abstract

The ability to control the morphologies of biomolecular aggregates is a central objective in the study of self-assembly processes. The development of predictive models offers the surest route for gaining such control. Under the right conditions, proteins will self-assemble into fibres which may re-arrange themselves even further to form diverse structures, including the formation of closed loops. In this study chicken egg white ovalbumin is used as a model for the study of fibril loops. By monitoring the kinetics of self assembly we demonstrate that loop formation is a consequence of end-to-end association between protein fibrils. A model of fibril formation kinetics including end-joining is developed and solved, showing that end-joining has a distinct effect on the growth of fibrillar mass density (which can be measured experimentally) establishing a link between self-assembly kinetics and the underlying growth mechanism. These results will enable experimentalists to infer fibrillar morphologies from an appropriate analysis of self-assembly kinetic data.

Submitted on October 3, 2014

*Correspondence: [CE MacPhee, SUPA, School of Physics and Astronomy, University of Edinburgh, Mayfield Road, Edinburgh EH9 3JZ, cait.macphee@ed.ac.uk]

INTRODUCTION

The self-assembly of polypeptides into fibrillar aggregates is relevant into areas as diverse as disease pathology (1) and the synthesis of bio-compatible nanomaterials (2, 3). The formation of "amyloid-like" fibrils, which are rich in β-sheet structure has been the focus of much research due to the universal nature of the self-assembly process: most if not all proteins can form amyloid-like fibrils under appropriate (not necessarily physiological) environmental conditions (4). The kinetics of amyloid fibril formation can be tracked using β sheet-binding dyes such as Congo red or Thioflavin T (Th T) or monitoring turbidity, while the morphology of the resulting fibrils can be assessed using electron microscopy. However these are usually measured in separate studies - few attempts have been made to link self-assembly kinetics to fibril morphology. Establishing such a link would be an important step forward in understanding, predicting and controlling protein aggregation processes.

The kinetics of amyloid-like fibril formation, as measured using spectroscopic assays such as the thioflavin T fluorescence assay (5–7), are typically characterised by growth curves of a sigmoidal or sigmoidal-like form, in which a quiescent lag phase - often lasting hours or even days - is followed by rapid growth, culminating in a plateau when monomeric protein is exhausted or the system reaches equilibrium. The lag phase can be abolished by adding preformed fibril "seeds", suggesting that a nucleation process plays a key role. Indeed, theoretical models that include nucleation, growth by monomer addition at fibril ends and autocatalysis via fibril fragmentation can successfully reproduce these sigmoid-like growth curves (8–10). Here the role of fibril fragmentation is to form new growth-competent fibril "ends" which accelerate the depletion of monomer during the growth phase, leading to the characteristic sigmoidal form for the fibril growth curve. These models also predict characteristic scaling laws for the lag time and maximal growth rate as functions of the protein concentration. An alternative protein aggregation process may exhibit rapid fibril growth from the very onset with an absence of lag phase - examples of this phenomenon are cited below.

0006-3495/08/09/2624/12 $2.00 doi: 10.xxxx/biophysj.xxx.xxxxxx

Amyloid fibrils have been observed to form in a wide variety of morphologies, including long rigid fibrils, short rod-like forms, wide tapes and flexible worm-like chains which are characterised by a shorter persistence length (1, 11). Fibril polymorphism may become manifest when the self-assembly takes place under different conditions, as seen for β2-microglobulin (12), or, alternatively, two forms may arise simultaneously, as observed for amyloid β (13, 14). Intriguingly, a number of systems that form fibres with worm-like chains have also been observed to form ring or loop structures (e.g. apolipoprotein C-II (16), α-synuclein (18), the crystallins (19, 20), human serum albumin (21), β-lactoglobulin (22) and α_{S2}-casein (23). The simplest hypothesis for the formation of loops by protein fibrils is joining of their two ends (24). This hypothesis implies a link to fibril growth kinetics, since end-joining decreases the number of fibril ends available for growth by monomer addition. In this study we show that such a link between end-joining and self-assembly kinetics indeed exists, using the 44.5kDa glycoprotein OVA, the main protein component of avian egg white, as a model system. Due to its abundance, OVA is a convenient model system for the study of fibril formation. Under acidic or near-neutral conditions (pH $\leq$ 7) and elevated temperatures, OVA forms fibrils that display amyloid-like behaviour in that they bind the dyes ThT and Congo Red (25–29) (SI Figures S1 and S2; Figure 3). The formation of amyloid-like fibrils is more pronounced when the reaction takes place in a reducing environment (30). Published images of OVA fibres indicate flexible morphologies (28), however under reducing conditions more rigid fibres have also been observed (30). We investigate in detail the self-assembly kinetics of OVA fibrils, under conditions where flexible fibrils, with some closed loops, are formed. We develop a theoretical model which includes both fibril fragmentation and the joining of fibril ends. By fitting our model to our experimental data, we show that both fragmentation and end-joining play important roles in the self-assembly kinetics.

MATERIALS AND METHODS

Preparation of Ovalbumin fibrils

Ovalbumin (isolated from chicken egg white) used in this study was purchased from Sigma (Grade 5; A5503). In order to produce reduced OVA samples, the lyophilised protein powder was dissolved in aqueous 10mM ammonium acetate 10 mM dithiothreitol buffer (pH 6.8), achieving the desired protein concentrations (ranging between 0.1 and 12.8 mg/ml). Subsequently, the sample, distributed in 1.2 mL aliquots in Eppendorf tubes secured with parafilm, was incubated on a benchtop block heater at 37°C for 2 hours. Reduced protein aliquots were mixed, cooled on ice and filtered with a 200 μm cutoff filter. Fibrils were produced by incubating the samples at 60°C. Incubation typically occurred in 96-well plates in the plate reader or on the block heater (in the latter case Eppendorf tubes were secured with parafilm).

Thioflavin T fluorescence kinetics at 60°C

Fibril formation kinetics were followed by means of the Th T fluorescence assay. Th T was added to reduced protein samples to a concentration of 55 μM. 100 μL aliquots were added in 96-well plates. Corning Non-Binding surface plates (coated with a PEG-like polymer) and Nunc-Immuno StarWell Modules (PolySorp surface; polystyrene coating), the latter sealed with polyethylene caps, were used for these experiments. Both plate types were sealed additionally with a transparent adhesive plate sealer (Greiner) and secured further with parafilm in order to minimise solvent evaporation. Typically 60 out of a total of 96 wells contained the protein solution with the remaining 36 being used for blanks. The kinetics were measured using a BioTek Synergy 2 plate reader. The microplate was kept at a temperature of 60°C for plate-reader measurements. Th T fluorescence readings ($\lambda_{\text{exc}} = 440$ nm, $\lambda_{\text{em}} = 485$ nm) were collected every 8 minutes, with a 18Hz shaking frequency (”medium” setting). Th T binding kinetics were probed for 3-5 days.

Temperature-dependence of Th T binding kinetics

The kinetics of Th T binding were measured on quiescent samples on a Varian Cary Eclipse fluorimeter, fitted with a Peltier device. 3.0 mL of 6.0 mg/mL reduced protein solution (prepared as described above) was added to 10mm-path quartz cuvettes (Starna Scientific). The kinetics were monitored for 24 hours, collecting a reading every 10 minutes. OVA Th T binding kinetics were measured at 50, 55, 60, 65, 70 and 80°C in this fashion. These experiments were repeated in triplicate, with buffer blanks being measured in duplicate.

Transmission Electron Microscopy

For TEM, 2.0 μL reduced OVA fibril suspension were deposited on formvar/carbon coated TEM grids (TAAB). The sample was allowed to equilibrate for 5 minutes after which the excess was removed with a filter paper wedge and washed with 20 μL of distilled H_2O, which was then immediately removed. The samples were stained with 1% w/v uranyl acetate. Staining time ranged between 30 and 45 s. Excess stain was removed and the grids were allowed to dry for at least 20 minutes prior to analysis.

TEM images were collected on a Phillips CM 120 Biotwin transmission electron microscope and captured by a Gatan Orius 1000 CCD camera controlled using DigitalMicrograph™ (Gatan, Inc., USA) imaging software. Image analysis was carried out using the *ImageJ* program.

Protein Quantitation

Whenever necessary, protein concentrations were determined using the Bradford assay. 10 μL of standard protein solution or fibril sample (appropriately diluted - 1,2,5 or 10× - in 10 mM NH_4CH_3COO 10 mM DTT buffer) were dissolved in 200 μL of Bradford reagent. The absorbance was recorded at 450 nm and 595 nm and the ratio of the two readings were used to construct the standard curve and to determine the concentrations. OVA was used as the protein standard, allowing accurate concentration determination.

Model for fibril formation by linear growth, end-joining and fragmentation

Our kinetic and morphological observations, presented in Results and Discussion, suggest that OVA fibril formation involves seeded linear fibril growth, combined with a secondary process, such as end-to-end joining, that can produce loops. Indeed, a kinetic model that includes seeded linear growth and end-joining (which can be solved analytically; see SI) does predict rapid fibril growth followed by saturation, similar to what we see in our experiments. However, this model does not reproduce the second, slower growth regime (Fig. S6); we find a good fit to the experimental data if we also include in the model fibril fragmentation - i.e., the generation of new fibril ends by breakage of growing fibrils (see Figure 5). This suggests that fragmentation is a significant factor in the self-assembly of OVA, even though its growth kinetics display none of the characteristics typically associated with fragmentation-based models.

A model for the self-assembly of fibrils which incorporates end-joining and loop formation can be summarised using the following reaction set, schematically presented in figure 1:

$$F_i + m \xrightarrow{k_+} F_{i+1} \quad [1]$$

$$F_i \underset{k_j}{\overset{k_f}{\rightleftharpoons}} F_{i-j} + F_j, \quad i,j \geq n_c \quad [2]$$

$$F_i^{\text{loop}} \underset{k_l}{\overset{k_f}{\rightleftharpoons}} F_i \quad [3]$$

Here, F_i is a single fibril of length i, m is a single monomer, n_c is the number of monomers in the smallest stable fibril (fibrils shorter than n_c are assumed to dissolve into monomers) and F_i^{loop} is a loop of size i. The total monomer concentration is denoted with $m(t)$. The first reaction describes the elongation of a fibril by addition of a monomer to either of its ends, with rate constant k_+. The second reaction describes the breakage of a fibril of length i at any point between two of its monomers with rate constant k_f; the opposite process of joining two fibril ends has rate constant k_j. The third reaction describes the breakage of a loop of length i in a similar way to that of a single fibril (N.B. a loop contains one more breakable bond than a fibril of the same length) with the same rate constant k_f; similarly, in the opposite process a loop is formed with rate constant k_l; this rate is given by k_j/V multiplied by the probability P_{loop} of two ends of a worm-like chain meeting together (16).

The rate equations for the mass density $M(t)$ and the number density $N(t)$ of fibrils may be written as:

$$\frac{dM}{dt} = 2k_+(m_{\text{tot}} - M)N - k_f n_c(n_c - 1)N, \quad M(0) = M_0 \quad [4]$$

$$\frac{dN}{dt} = k_f[M - (2n_c - 1)N] - k_j N^2, \quad N(0) = N_0, \quad [5]$$

where m_{tot} represents the total density of protein monomers; N_0 and M_0 are the initial ("seed") fibril number density and fibril mass concentration respectively. Equations ([4])-(5) were derived from the master equation for the number density of fibrils of sizes $i \geq n_c$ (see Supplemental Material).

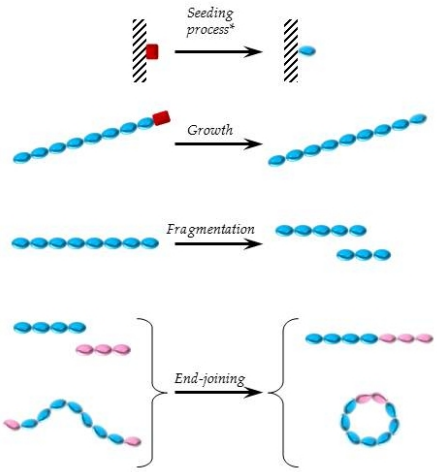

Figure 1: Schematic representation of processes described by the model of reactions (1)-(3), which are also thought to take place during OVA self-assembly. The process giving rise to the initial seed population is not defined explicitly and instead is modelled by the presence of a seed population that forms rapidly at early times.

Solving for the steady state of the set of equations (4)-(5) provides an expression for the fibril mass concentration M^* and number density N^*, in the long-time limit:

$$M^* = m_{\text{tot}} - \frac{k_f n_c (n_c - 1)}{2k_+} \quad [6]$$

$$N^* = \frac{\sqrt{k_f^2 (2n_c - 1)^2 + 4k_j k_f M^*} - k_f (2n_c - 1)}{2k_j}. \quad [7]$$

The dynamical trajectories leading to the state (M^*, N^*) provide predictions for the self-assembly kinetics. These trajectories can be obtained analytically in an approximate form (assuming small k_f and sufficiently large N_0), or using numerical simulations, both of which are described in the following sections.

Analytical solution for the self-assembly kinetics of a model including monomer addition, fragmentation and end-joining

An approximate solution for the set of equations (4) and (5) can be obtained in closed form using the following method, for the choice of parameters for which $m(t)$ does not develop a sigmoidal shape; a closed form solution for the case where $m(t)$ develops a sigmoidal shape has been obtained very recently in (17).

First, it is useful to define $m = M/M^*$ and $n = N/N^*$, so that the equation is now expressed in terms of the dimensionless ratio of fibril mass and number density relative to their steady state value. After rescaling the time variable $\tau = 2k_+ N^* t$, and assuming $k_f \ll k_+ m_{\text{tot}}$ and $k_f \ll k_j m_{\text{tot}}$, the system (4)-(5) can be written as

$$\frac{dm}{d\tau} = (1 - m)n, \quad m(0) = M_0/M^* = m_0 \quad [8]$$

$$\frac{dn}{d\tau} = -rn^2 + rm, \quad n(0) = N_0/N^* = n_0, \quad [9]$$

where $r \equiv k_j/(2k_+)$ is the ratio of the end-joining to the elongation rate constants. Equation (8) can be integrated yielding an expression for $m(\tau)$ given an expression for $n(\tau)$

$$m(\tau) = 1 - (1 - m_0) e^{-\int_0^\tau d\tau' n(\tau')}. \quad [10]$$

At late times $n \approx 1$ yielding

$$m(\tau | n \to 1) = 1 - (1 - m_0) e^{-\tau}. \quad [11]$$

$m(\tau|n \to 1)$ is a monotonically increasing, concave function and thus may serve as a good approximation to $m(\tau)$ at early times provided $m(\tau)$ does not develop a sigmoidal shape. Using this expression as an approximation for $m(\tau)$ at early times, we obtain the following non-linear 1st order ODE for $n(\tau)$:

$$\frac{dn}{d\tau} = -rn^2 + r - r(1-m_0)e^{-\tau}, \quad n(0) = n_0. \qquad [12]$$

This equation can be solved (see SI for details):

$$n(\tau) = \frac{u}{4r}\frac{c[J_{2r+1}(u) - J_{2r-1}(u)] + Y_{2r+1}(u) - Y_{2r-1}(u)}{cJ_{2r}(u) + Y_{2r}(u)}, \qquad [13]$$

$$u = 2r\sqrt{1-m_0}e^{-\tau/2} \qquad [14]$$

$$c = \frac{Y_{2r-1}(2r\sqrt{1-m_0}) - Y_{2r+1}(2r\sqrt{1-m_0}) + \frac{2n_0}{\sqrt{1-m_0}}Y_{2r}(2r\sqrt{1-m_0})}{J_{2r-1}(2r\sqrt{1-m_0}) - J_{2r+1}(2r\sqrt{1-m_0}) + \frac{2n_0}{\sqrt{1-m_0}}J_{2r}(2r\sqrt{1-m_0})}, \qquad [15]$$

$J_\alpha(x)$ and $Y_\alpha(x)$ being Bessel functions of the first and second kind respectively. Expression (13) can be integrated and combined with (10) to obtain the following approximation for $m(\tau)$:

$$m(\tau) = 1 - (1-m_0)\left(\frac{cJ_{2r}(2r\sqrt{1-m_0}) + Y_{2r}(2r\sqrt{1-m_0})}{cJ_{2r}(2r\sqrt{1-m_0}e^{-\tau/2}) + Y_{2r}(2r\sqrt{1-m_0}e^{-\tau/2})}\right)^{1/r}, \qquad [16]$$

where the constant c is as defined in (15). Plots of the approximate solution given by (13) and (16) are shown in Figure S5 along with curves generated numerically; clearly the agreement between them is excellent.

An expression relating m and n may also be derived from (8)-(9):

$$n\frac{dn}{dm} = -\frac{r}{1-m}n^2 + \frac{rm}{1-m}. \qquad [17]$$

This is solvable for any n_0, r and m:

$$n(m) = \begin{cases} \left[\left(n_0^2 - \frac{2rm_0-1}{2r-1}\right)\left(\frac{1-m}{1-m_0}\right)^{2r} + \frac{2rm-1}{2r-1}\right]^{1/2}, & r \neq 1/2, \\ \left[\left(n_0^2-1\right)\frac{1-m}{1-m_0} + (1-m)\ln\frac{1-m}{1-m_0} + 1\right]^{1/2}, & r = 1/2. \end{cases} \qquad [18]$$

This is an exact implicit solution that relates the fibril number and fibril mass densities.

Simulation of the self-assembly process including end-joining

Kinetic (stochastic) Monte Carlo simulations were performed by implementing Gillespie algorithm using Fortran 95 and then by averaging over 150 replicate simulations for each set of conditions. The number of loops and fibrils were tracked for each of length, along with the total monomer population $m(t)$. Length distributions were obtained at points in the simulation where the total fibril mass had reached a specific threshold (i.e. instead of at particular points in time).

RESULTS AND DISCUSSION

Heat treatment of reduced OVA produces fibrillar aggregates and closed loops with amyloid-like Congo Red and Thioflavin T binding properties

Incubation of reduced (10 mM DTT) OVA for several hours at 60°C at near-neutral pH (10 mM ammonium acetate, pH 6.8) produced species which bound Congo red (see SI figure S1) and Th T. Examination of the heated OVA samples by TEM revealed the presence of fibrillar aggregates (Figure 2 A-C). The fibrils formed by reduced OVA under these conditions are flexible with a persistence length of approximately 26 nm (see Fig. S2 in the supplemental material). The fibrils often appeared to be entangled, particularly at higher protein concentrations, a feature that prevents an accurate determination of their length distribution. Interestingly, our TEM images often reveal the formation of loops, in which the two ends of a single fibril appear to be annealed. Loops were observed in TEM images of heat-treated samples at both low (0.4 mg/ml) and high (6.4 and 12.8

mg/ml) initial concentration of protein (Fig. 2 A-D). The presence of loops in the samples provides clear evidence that fibrils of length greater than the persistence length can join end-to-end. Analysis of images from samples in which loop formation was abundant ($80°C$, 6.4 mg/ml) showed that the length distribution of fibrils in loops is centred at 120 nm, but skewed towards longer loops (loops as large as 360 nm in circumference could be seen; see histogram in Fig. 2 E). No loops were seen with circumference smaller than twice the persistence length, the smallest measured loop having a length of 74 nm.

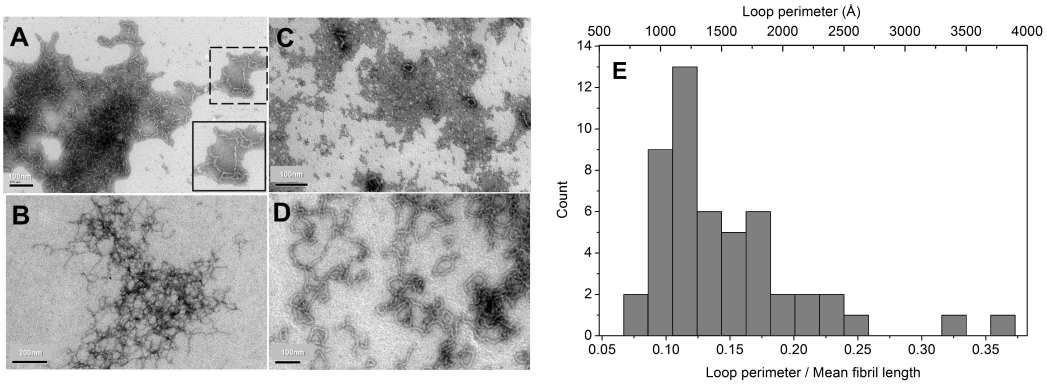

Figure 2: TEM images of fibrils formed by OVA along with branching angle and fibril diameter distributions. A) Entangled and branched fibrils formed by 0.4 mg/ml OVA heated at 60°C. Inset shows an example of a branched fibril. B) Entangled and branched fibrils formed by 12.8 mg/ml OVA heated at 60°C. C) Loops formed by 0.4 mg/ml OVA fibrils at 60°C. D) Loops formed by 6.4 mg/ml OVA fibrils at 80°C. E) Experimental length distributions of OVA (6.4 mg/ml, incubated at 80°C) loops.

The kinetics of OVA self-assembly

The self-assembly kinetics of reduced OVA differs strongly from the standard sigmoidal behaviour, and can be divided into three regimes (Figure 3 A). In our experiments, fibril mass, as measured by the ThT fluorescence, increases sharply from the start of the experiment, with no apparent lag phase (although at very early times, our measurements are obscured by a transient behaviour that we attribute to temperature fluctuations). This initial growth phase is followed by a second growth regime, where the ThT fluorescence continues to increase but considerably more slowly, following which, the ThT fluorescence reaches a plateau.

The absence of a lag phase suggests that fibril formation in our experiments does not proceed via a classic homogeneous nucleation and growth mechanism by monomer addition. This interpretation is supported further by measurements of the relationship between protein concentration and the initial growth rate (Figure 3 B). For a mechanism involving homogeneous nucleation and growth, one would expect that the initial aggregation rate, in the absence of seeds, to be equal to the initial nucleation rate, which can be assumed to scale as [protein concentration]^{n_c} (for rate-limited reactions), $n_c \geq 2$ being the size of the nucleus. However, as shown in Figure 3 B, in our experiments the initial aggregation rate scales linearly with protein concentration, suggesting that a process other than homogeneous nucleation must give rise to the initial population of growth-competent species. We also noticed that the initial aggregation rate was influenced by the material of the vessel in which our experiments were performed, with aggregation in microplates coated with a PEG-like polymer occurring substantially faster than in uncoated plates (see SI for details). The initial aggregation rate also depends on the volume of the sample, with samples with a smaller surface area to volume ratio exhibiting less growth (see Figure S3 D-E). These findings suggest that fibril growth is seeded at the walls of the sample container. For seeded growth, the initial growth rate is controlled by the initial monomer addition rate, which scales linearly with number of seeds and protein concentration. If the surface is saturated with fibril seeds, then the number of seeds is independent of protein concentration, which would give rise to the observed linear scaling of the initial rate with protein concentration.

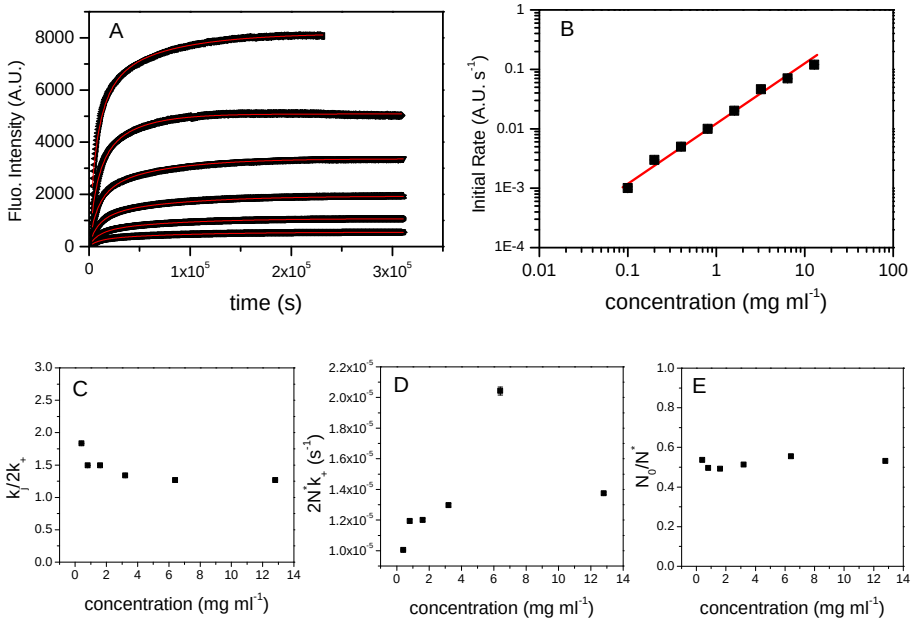

Figure 3: OVA self-assembly kinetics monitored by thioflavin T binding. A) Kinetic traces of ThT binding by OVA between 0.4-12.8 mg/ml. Symbols represent the experimental data; fitted curves according to equation (16) are shown as red solid lines. B) log-log plot of the initial growth rate vs. concentration (red line represents a linear scaling relation). C) Concentration dependence of the ratio of end-joining and growth rate constants. Interestingly, this factor decreases with concentration, possibly reflecting the lower diffusivity of the initial seed population in concentrated mixtures (which may arise since the effect of fibril length on growth is not taken into account by the model). D) Concentration dependence of the time-scaling factor $2k_+N^*$. While this factor increases with concentration, the observed dependence is much weaker than the one predicted from the theory (Eq. 7). E) Concentration dependence of the ratio N_0/N^*. Since N^* is only weakly dependent on concentration, a constant ratio of $N_0/N^* \approx 0.5$ predicts that N_0 is concentration independent, a necessary condition for the model to be consistent with the linear concentration scaling of the initial rate (B).

Theoretical analysis of the model for fibril formation by linear growth, end-joining and fragmentation

Results for the theoretical trajectories of the model described by equations (8)-(9) reveal qualitatively different types of dynamical behaviour, depending on the parameters - in particular on the initial concentration of seed fibrils N_0 (see the phase diagram shown in Figure 3 A).

For small seed density $N_0 \ll N^*$ (i.e. if the initial concentration of seeds is much smaller than the long-time fibril density), the model predicts sigmoidal kinetics for the fibril mass M. In this case, the only apparent effect of end-joining is to smooth out the transition between the rapid growth phase and the plateau (Figure 4 B and C, $n_0 = 0.001$). By taking the kinetics of the fibril number density $N(t)$ into account, we may distinguish two cases: if the end-joining rate constant is much less than the elongation rate constant, i.e. $k_j \ll 2k_+$, $N(t)$ increases slowly as the bulk of the free protein aggregates, increasing sharply to its long-time value during the late stages of the process (Figure 4 C, $r = 0.1$). When k_j is comparable to or greater than $2k_+$, $N(t)$ follows a sigmoidal form similar to $M(t)$ (Figure 4 C, $r = 2$).

Contrasting behaviour is predicted by the model if the initial seed concentration is sufficiently high. In this case, the model predicts rapid fibril growth from the start, with no lag phase (figure 4 B, $n_0 = 1.5$). For a small end-joining rate $k_j \ll 2k_+$, $M(t)$ shows a single growth phase, ending in a plateau, while $N(t)$ decays monotonically to its long-time value N^* (Figures 4 B and C, $r = 0.1$). Interestingly however, if the end-joining rate constant is significant ($k_j \simeq 2k_+$), the model predicts two distinct fibril growth phases: the fibril mass concentration $M(t)$ initially grows rapidly, followed by a slower growth phase, before it eventually reaches a plateau. This behaviour is correlated with the kinetics of the fibril number $N(t)$, which is non-monotonic: $N(t)$ decreases during the initial growth phase, overshoots its long-time value N^* and gradually increases towards N^* during the second fibril growth phase (Figure 4 C, $r = 2$).

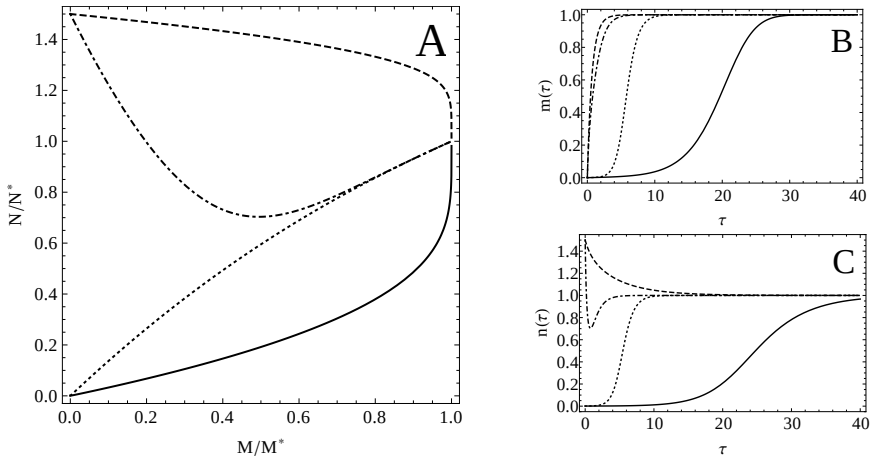

Figure 4: Theoretical trajectories of the model described by equations (8)-(9). A) Phase diagram of the system showing four distinct types of dynamics: [———] small initial seed population and small end-joining rate ($n_0 = 0.001, r = 0.1$); [·····] small initial seed population and end-joining rate comparable to elongation ($n_0 = 0.001, r = 2$); [- - - -] high initial seed population and low end-joining rate ($n_0 = 1.5, r = 0.1$); [–·–·–] high end-joining rate and high initial seed population ($n_0 = 1.5, r = 2$). The dynamics of the normalised fibril mass density m and the normalised fibril number density n for these four cases are shown in panels (B) and (C), respectively. When the end-joining rate constant is comparable to the elongation rate constant and the initial seed concentration is also high, fibril growth sites are depleted at early times due to end-joining of fibril ends before they begin increasing again at later times as a result of fibril breaking; this fluctuation generates a characteristically delayed equilibration of the fibrillar mass fraction growth curve.

The bi-phasic aggregation kinetics predicted by the model is strikingly similar to our experimental observations for OVA. Therefore, the model leads us to suggest not only that both fragmentation and end-joining are important for OVA, but also that in our experiments self-assembly starts with a large number of short but growth-competent species, which due to their small size may still represent a very small proportion of the total mass fraction. The model also predicts that the absolute number of fibrils in our experiments (as opposed to the fibril mass) actually decreases in time from its initially high value, before again increasing.

Thus our theoretical analysis suggests that the kinetics observed in our experiments reflect the interplay between the two competing processes of fragmentation (which creates new growth-competent ends) and end-joining (which decreases the number of fibril ends). Initially, growth proceeds rapidly from a seed population that consists of numerous small species. Later, a relatively high rate of end-joining depletes the number of fibril ends to which free monomers may attach: this process is manifested by the decrease in the growth rate which is evident in the second observed growth phase. Finally, a small fibril breakage rate eventually ensures there are enough ends for the remaining free monomers to attach to, bringing the fibril growth process to completion.

Experimental confirmation of the growth pathway

Fitting our experimental ThT fluorescence curves for ovalbumin (Fig. 3) using our analytical formula (Eq. 16) for the self-assembly kinetics including end-joining and fragmentation allows us to estimate the relevant kinetic parameters (Fig. 3 C-E). The initial number density of fibril seeds (i.e. growth-competent species) is indeed estimated to be high ($N_0/N^* \approx 0.5$, Fig. 3 E), but these seeds nonetheless represent only a very small proportion of the total amount of protein present ($M_0 \ll m_{tot}$). Interestingly, the rate constants for elongation and end-joining are of similar magnitudes (Fig. 3 C), suggesting that end-joining is of comparable importance to the kinetics. As can be seen in Fig. 3 D, the time-scale factor $2k_+N^*$ increases with concentration, but the observed dependence is weaker than predicted from the theory (Eq. 7). This, together with the observation that the ratio N_0/N^* is a constant (Fig. 3 E), implies that N_0 is concentration independent and is consistent with our previous argument that fibril seeds are saturated at surfaces.

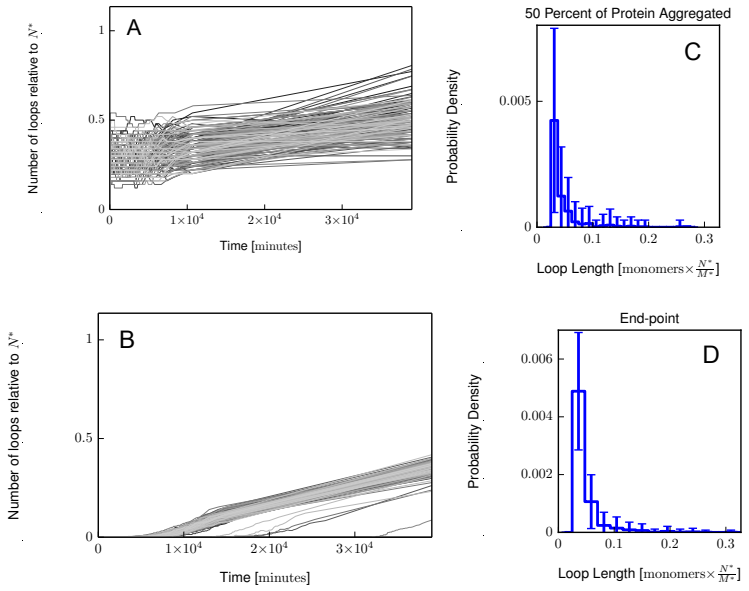

Figure 5: The dynamics for the loop number fraction generated by stochastic simulations for A) heavily seeded growth and B) for a case exhibiting sigmoidal kinetics. Thin lines represent individual runs, the thick yellow line the ensemble average. We find that the number of loops is established early in the kinetics for highly seeded growth. This is in contrast to low initial seed concentrations where the appearance of loops does not happen until further into the growth kinetics and does not reach an appreciable number until late times. C) Simulated loop perimeter distribution at the mid-point; D) simulated loop perimeter distribution at the end-point. Both simulated distributions are normalised to the average fibril length at equilibrium.

Having all the relevant parameters in hand, we can perform a simulation of the model using the parameters derived from fitting of the experimental data, which allow us to monitor evolution of species over time. Due to the high number of fibrils forming early during polymerisation, we observe loops forming rapidly during the early stages (Figure 5 A), and then increasing at a diminishing rate. This gives rise to a loop length distribution that increases fairly sharply at lengths greater than $2l_p$ and then decays more slowly with increasing loop length (Figure 5 C & D). The length distribution for loops is thus qualitatively similar with the one observed experimentally, i.e. peaked but with a long tail (Figure 2 E). This loop perimeter distribution is established early (when less than 50% of the starting material has aggregated) and does not change significantly over time. Therefore, it may be expected that in systems with flexible fibrils with sufficiently high initial seeding species the loop population will have formed after the initial growth phase and remain intact until the process is completed. This situation can be contrasted with the curves displaying sigmoidal kinetics (resulting from small initial seed concentrations) where loops only appear after some lag-time and only reach an appreciable number when the self-assembly process is almost complete (Figure 5 B). The model studied in this paper therefore provides a framework for predicting when different fibril morphologies arise.

It is also worth commenting on the observation that OVA fibrils exhibit branched morphologies (inset to 2 A). We can show that these branches do not form by fibrils overlapping on the surface of the TEM grid as an artifact of the deposition process by analysing the angular distribution of the fibril branches (Figure S4). Such branching may occur via two different mechanisms: heterogeneous nucleation at a fibril surface or joining of an existing fibril end to the body of another fibril. Kinetically, these processes are distinct. Heterogeneous nucleation will be a source of new fibril ends, whereas annealing of an existing fibril end to the body of another fibril will act as a sink by consuming one growth-competent end. Our kinetic analysis is consistent with a model where fibril ends are depleted rather than created during the aggregation process, suggesting that the joining of an existing fibril to the body of another occurs during OVA self-assembly under these conditions.

The fact that the rate constants for elongation and end-joining are of similar magnitudes may be due to the flexibility of the fibrils - for flexible fibrils the correlations between the fibril mass and diffusion of ends dies out relatively quickly; as such, they may be seen as free-floating particles which react with each other in a manner similar to how they react with monomers. This may suggest that joining of fibril ends and elongation have similar activation barriers. Such a result is plausible since both processes involve protein-protein assembly.

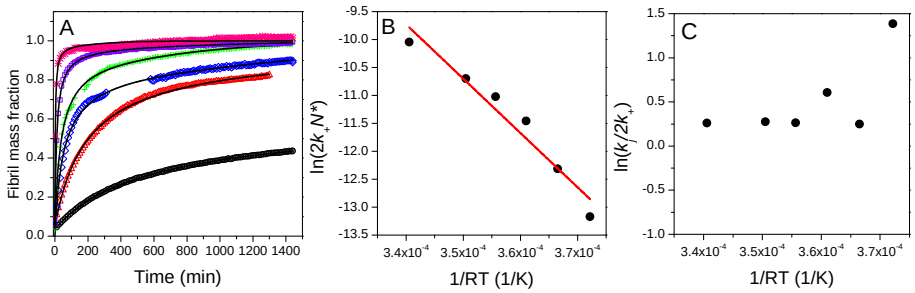

Figure 6: A) Kinetic traces of Th T binding by 6.0 mg/ml OVA at 50 (black circles), 55 (red triangles), 60 (blue diamonds), 65 (green +), 70 (purple squares) and 80°C (pink *). Symbols represent experimental data; fitted curves are shown as black solid lines. B) Arrhenius plot for the time scaling factor $2k_+N^*$ for 6.0 mg/ml OVA. C) Arrhenius plot for the $k_j/(2k_+)$ ratio for 6.0 mg/ml OVA. Clearly the latter does not exhibit typical Arrhenius behaviour, indicating that end-joining and elongation have similar energy barriers.

Analysis of OVA fibril growth kinetics at different temperatures supports this hypothesis (Figure 6 A-C). ThT fluorescence during the assembly of OVA at a concentration of 6.0 mg/ml was recorded at six different temperatures (50, 55, 60, 65, 70, and 80°C). As expected, the fibril formation process is accelerated at higher temperatures. Arrhenius plots show that the ratio $r = k_j/(2k_+)$ (see Methods) remains essentially constant with temperature (Figure 6 C), suggesting that end-joining and elongation have similar activation barriers. This result can easily be understood by first assuming an Arrhenius-like form for the relevant rate constants, i.e., $k_j = Ae^{-(E_j^\dagger/RT)}$ and likewise for k_+. Since our experiments have shown that $\frac{d(lnr)}{d(1/RT)} \approx 0$, it follows then that $E_j^\dagger \approx E_+^\dagger$. Conversely, $2k_+N^*$ does display Arrhenius behaviour (Figure 6 B). Since, for $k_f \ll k_+, k_j$, N^* can be approximated by $(m_{tot}k_f/k_j)^{1/2}$, the gradient of the Arrhenius plot $\frac{d(ln[2k_+N^*])}{d(1/RT)} \approx -E_+^\dagger - \frac{1}{2}E_f^\dagger + \frac{1}{2}E_j^\dagger$, where $E^\dagger$ represent activation energies for each process. The energy barrier obtained from Figure 6 B is 97.2 kJ/mol. The similarity of the energy barriers for end-joining and fibril growth are interesting and may point to these two processes being mechanistically similar, *i.e.*, that a strong parallel may exist between monomer addition at a growth site and the coalescence of two fibril growth sites. Moreover, as the polymerisation rate changes visibly over the temperature range studied (as evidenced by Figure 6 A) the energy barrier ought to be comparable to RT at that temperature range (2.7-3.1 kJ/mol), assuming that these processes are rate-limited. Thus, by far the major contribution to the value obtained from Figure 6 B must originate from the fragmentation process. These considerations lead to an estimate of 191.2-191.8kJ/mol for $E_f^\dagger$ which is high compared to RT, a result that is entirely consistent with the initial assumption that fragmentation is a slow process. The initial fibrillar mass fraction does not display any trend as a function of temperature - indeed the fits allow significant variation for this parameter, given that it is a small number. Notably, temperature does affect the initial seed density with higher temperatures giving rise to a higher initial seed concentration; thus, whatever the seeding process is, it is temperature-dependent. Nevertheless, even samples incubated at 50°C do not display a measurable lag phase, indicating that the initial number of seeds never falls below the threshold value required for an appreciable lag phase to be observed.

The effect of end-joining on self-assembly dynamics and implications for amyloid-like fibril growth

Our model of ovalbumin self-assembly establishes a link between subtle features of the aggregation kinetics and the molecular processes underlying self-assembly: in this case the joining between fibril ends. Such processes give rise to the formation of nano- and micro-scale structures with intriguing morphologies (e.g. loops). Such a model can also be enlisted to interpret a far wider array of self-assembly phenomena. In the limit of a vanishing end-joining term and a low seed concentration, the kinetics approach the nucleation, growth and fragmentation model, which begins with a lag phase but is followed by fast growth, equilibrating rapidly due to its autocatalytic nature (8, 9). Polymerisation with low initial seed concentration and an end-joining term which effectively cancels out a small fragmentation term qualitatively resembles the classical “nucleation and growth” case, characterised by a short lag phase followed by a growth phase but with slow equilibration (34). When the end-joining term is sufficiently high it will effectively inhibit the polymerisation process by removing elongation sites. By counter-acting the effects of fibril fragmentation, inclusion of end-joining gives rise to kinetic curves that can have either

abrupt (small end-joining rate constant) or slow (large end-joining rate constant) equilibration following the growth phase. The fibril length distribution at late times resulting from this case is exponential, a hallmark of polymer fragmentation (35), but significantly broadened, indicating that end-joining dynamically stabilises large aggregates (see Figure 3 C,E). Thus the simple inclusion of an end-joining term to the equations describing linear polymerisation and fibril breaking can significantly improve the quantitative understanding of protein fibrillisation (and other similar polymerisation reactions) as well as describing processes, such as those observed for OVA, which cannot be accounted for without it.

The model described by equations (4)-(5) and its solutions (equations (16) as well as (S22) and (S35) can be used to reveal if end-joining and fragmentation contribute significantly to a fibrillisation process based on the aggregation kinetics. In doing so, several new questions are opened up. What are the molecular processes that allow end-joining to occur, which may explain the apparent values of the rate constants? The fact that the systems under question grow linearly into fibrils implies that there exists a preferred direction for growth (at least once a sufficiently large oligomer has already formed); but can anything be said about the arrangement of the peptides in the fibril core? In straight amyloid-like fibrils, peptide strands are thought to exist in a highly ordered, quasi-crystalline state (36, 37). Such an arrangement limits the number of orientations in which another fibril end may "dock" to an existing end, unless monomers at fibril ends initially have a different configuration before they adopt that of the fibril interior. Alternatively, the interface between monomers in a fibril may exhibit some structural heterogeneity, which might, in turn, explain both high end-joining and elongation rates but also the flexibility of the resulting fibres, observed not only for OVA but for other aggregating proteins (38–40). Thus, end-joining (and possibly elongation) must either be a multi-stepped processes ("dock and lock"), or a certain degree of structural variability should be expected along the fibril.

Several proteins form polymorphic fibrils. Some form different fibril morphologies under different environmental conditions (such as in apo-C II (41), a-syn (39, 40), β-2m (12) and OVA (31, 32)). Alternatively some, like Aβ, form flexible, worm-like fibrils early in the aggregation process before the appearance of rigid fibrils (9). As with OVA, in several other cases end-joining is implied by the presence of loops (16, 18–23). Notably, aggregation leading to the formation of worm-like fibrils will often either exhibit a short lag phase, or not exhibit a lag phase at all, indicating that the process giving rise to the critical concentration of growth-competent species is rapid: is this situation brought about by the inherent stability of the nucleus for worm-like fibrils or is it a result of worm-like fibrils being able to grow from a heterogeneous mix of monomer conformations?

Another question, of relevance to the role of amyloid-like fibrils in disease, concerns the toxicity of the fibril population resulting from this mechanism (which has also been raised by Hatters *et al.* (16)). In the long-time limit, assuming that the fibrils do not undergo any further rearrangements, the fibril length distribution will be broad but exponential. For flexible fibrils, and even with the inclusion of fibril fragmentation, short loops will be present from the initial growth phase onwards (Figure 5). The consequences of such a fibril length distribution are determined by whether shorter fibrils are cytotoxic. If they are then it may be expected that the formation of loops will stabilise toxic species, since short loops are indeed very stable (as they cannot grow any further and their breaking is relatively infrequent due to their small length which limits the number of possible breakage sites). Intriguingly, closed loops have been shown to form by aggregating α-synuclein (18); furthermore shorter fibrils formed by fragmentation of larger amyloid fibrils have been found to be more cytotoxic for a number of systems, including α-synuclein (42). Thus the stabilisation of short species by circularisation could prove detrimental if such aggregates are cytotoxic. However, if protein oligomers rather than fibrillar aggregates are the toxic species, loop formation would be desirable as it would lock away the constituent proteins in an inert state for an extended time period; thus, a method of inducing fibril end-joining would delay the accumulation of toxic species. Thus, relating fibril morphology to the growth pathway can contribute to rationalising therapeutic strategies for amyloidoses.

Summary of solutions to fibrillar growth kinetic models involving end-to-end joining

Model	Solution	Comments
$dM/dt = 2k_+(m_{\text{tot}} - M)N$ $dN/dt = -k_j N^2$	$M(t) = m_{\text{tot}} - \frac{m_{\text{tot}} - M_0}{(1+k_j N_0 t)^{2k_+/k_j}}$	exact solution for the fibrillar mass density $M(t)$
	Eq. (18)	exact implicit solution $N(M)$, valid for any combination of parameters
$dM/dt = 2k_+(m_{\text{tot}} - M)N$ $dN/dt = k_f M - k_j N^2$	$M(t) = m_{\text{tot}} - \frac{m_{\text{tot}} - M_0}{1 - \frac{M_0}{m_{\text{tot}}} + \frac{M_0}{m_{\text{tot}}}\cosh(2k_+ N^* t) + \frac{N_0}{N^*}\sinh(2k_+ N^* t)}$	exact solution for $M(t)$, valid when $k_j = 2k_+$
	Eq. (16)	approximate solution for $M(t)$, valid when the kinetics are reminiscent of decay profiles, lacking a measurable lag phase

Table 1: M is concentration of monomer incorporated in fibrils (fibril mass density) at any time; N is concentration of fibrils (number density); M_0 is initial fibril mass density; N_0 is initial number density of fibrils; m_{tot} is total monomer density; $N^* \approx \sqrt{k_f m_{\text{tot}}/k_j}$ is equilibrium number density of fibrils; k_+ is linear growth rate constant; k_j is end-joining rate constant; k_f is fibril fragmentation rate constant.

Author Contributions

JMDK designed experiments, performed experiments, analysed data, and wrote the manuscript. JSN built and solved the mathematical model and wrote and edited the manuscript. RJM designed experiments, performed experiments, analysed data, wrote and edited the manuscript. KE designed, performed and analysed stochastic simulations. SC, ST and JG both performed experiments and analysed data. PEB, RJA and CEM designed the research and edited the manuscript.

ACKNOWLEDGMENTS

JSN, RJM, and CEM would like to acknowledge funding from EPSRC under grant number EP/J007404/1. JMDK and PEB also acknowledge funding by BBSRC under grant BB/C00759X/2. RJA was supported by a Royal Society University Research Fellowship.

References

[1] Chiti, F., and C. M. Dobson. 2006. Protein misfolding, functional amyloid, and human disease. Annual Review of Biochemistry 75:333-366.

[2] Cherny, I., and E. Gazit. 2008. Amyloids: Not only pathological agents but also ordered nanomaterials. Angewandte Chemie-International Edition 47:4062-4069.

[3] Channon, K., and C. E. MacPhee. 2008. Possibilities for 'smart' materials exploiting the self-assembly of polypeptides into fibrils. Soft Matter 4:647-652.

[4] Goldschmidt, L. T. 2010. Identifying the amylome, proteins capable of forming amyloid-like fibrils. Proc. Nat. Acad. Sci. USA. 107(8):3487-3492.

[5] Vassar, P. S., and C. F. Culling. 1959. Fluorescent stains, with special reference to amyloid and connective tissues. Arch Pathol 68:487-498.
[6] Saeed, S. M., and G. Fine. 1967. Thioflavin-T for amyloid detection. Am J Clin Pathol 47:588-593.
[7] Naiki, H., K. Higuchi, M. Hosokawa, and T. Takeda. 1989. Fluorometric-Determination of Amyloid Fibrils *In vitro* Using the Fluorescent Dye, Thioflavine-T. Anal Biochem 177:244-249.
[8] Cohen, S. I. A., M. Vendruscolo, C. M. Dobson, and T. P. J. Knowles. 2011. Nucleated polymerization with secondary pathways. II. Determination of self-consistent solutions to growth processes described by non-linear master equations. Journal of Chemical Physics 135(6):065106.
[9] Cohen, S. I. A., M. Vendruscolo, M. E. Welland, C. M. Dobson, E. M. Terentjev, and T. P. J. Knowles. 2011. Nucleated polymerization with secondary pathways. I. Time evolution of the principal moments. Journal of Chemical Physics 135:065105.
[10] Knowles, T. P. J., C. A. Waudby, G. L. Devlin, S. I. A. Cohen, A. Aguzzi, M. Vendruscolo, E. M. Terentjev, M. E. Welland, and C. M. Dobson. 2009. An Analytical Solution to the Kinetics of Breakable Filament Assembly. Science 326:1533-1537.
[11] Rochet, C.-J. and P. T. Lansbury. 2000. Amyloid Fibrillogenesis: themes and variations. Curr. Op. Struct. Biol. 10(1):60-68.
[12] Aggeli, A., M. Bell, L. M. Carrick, C. W. G. Fishwick, R. Harding, P. J. Mawer, S. E. Radford, A. E. Strong, and N. Boden. 2003. pH as a trigger of peptide β-sheet self-assembly and reversible switching between nematic and isotropic phases. Journal of the American Chemical Society 125:9619-9628.
[13] Harper, J. D., C. M. Lieber, and P. T. Lansbury. 1997. Atomic force microscopic imaging of seeded fibril formation and fibril branching by the Alzheimer's disease amyloid-β protein. Chemistry & Biology 4:951-959.
[14] Harper, J. D., S. S. Wong, C. M. Lieber, and P. T. Lansbury. 1997. Observation of metastable Aβ amyloid protofibrils by atomic force microscopy. Chemistry & Biology 4:119-125.
[15] Harper, J. D., S. S. Wong, C. M. Lieber, and P. T. Lansbury. 1999. Assembly of A$beta$ amyloid protofibrils: An in vitro model for a possible early event in Alzheimer's disease. Biochemistry 38:8972-8980.
[16] Hatters, D. M., C. A. MacRaild, R. Daniels, W. S. Gosal, N. H. Thomson, J. A. Jones, J. J. Davis, C. E. MacPhee, C. M. Dobson, and G. J. Howlett. 2003. The circularization of amyloid fibrils formed by apolipoprotein C-II. Biophysical Journal 85:3979-3990.
[17] Michaels, T.C.T. and T.P.J. Knowles. 2014. Role of filament annealing in the kinetics and thermodynamics of nucleated polymerization. Journal of Chemical Physics 140:214904.
[18] Conway, K. A., S. J. Lee, J. C. Rochet, T. T. Ding, R. E. Williamson, and P. T. Lansbury. 2000. Acceleration of oligomerization, not fibrillization, is a shared property of both α-synuclein mutations linked to early-onset Parkinson's disease: Implications for pathogenesis and therapy. Proceedings of the National Academy of Sciences of the United States of America 97:571-576.
[19] Meehan, S., T. P. Knowles, A. J. Baldwin, J. F. Smith, A. M. Squires, P. Clements, T. M. Treweek, H. Ecroyd, G. G. Tartaglia, M. Vendruscolo, C. E. MacPhee, C. M. Dobson, and J. A. Carver. 2007. Characterisation of amyloid fibril formation by small heat-shock chaperone proteins human α A-, α B- and R120G α B-Crystallins. Journal of Molecular Biology 372:470-484.
[20] Ecroyd, H., and J. A. Carver. 2009. Crystallin proteins and amyloid fibrils. Cellular and Molecular Life Sciences 66:62-81.
[21] Juarez, J., P. Taboada, and V. Mosquera. 2009. Existence of Different Structural Intermediates on the Fibrillation Pathway of Human Serum Albumin. Biophysical Journal 96:2353-2370.
[22] Jordens, S., J. Adamcik, I. Amar-Yuli, and R. Mezzenga. 2011. Disassembly and Reassembly of Amyloid Fibrils in Water-Ethanol Mixtures. Biomacromolecules 12:187-193.
[23] Thorn, D. C., H. Ecroyd, M. Sunde, S. Poon, and J. A. Carver. 2008. Amyloid fibril formation by bovine milk αs2-casein occurs under physiological conditions yet is prevented by its natural counterpart, αs1-casein. Biochemistry 47:3926-3936.
[24] Binger, K. J., C. L. L. Pham, L. M. Wilson, M. F. Bailey, L. J. Lawrence, P. Schuck, and G. J. Howlett. 2008. Apolipoprotein C-II amyloid fibrils assemble via a reversible pathway that includes fibril breaking and rejoining. Journal of Molecular Biology 376:1116-1129.
[25] Naeem, A., T. A. Khan, M. Muzaffar, S. Ahmad, and M. Saleemuddin. 2011. A Partially Folded State of Ovalbumin at Low pH Tends to Aggregate. Cell Biochem Biophys 59:29-38.
[26] Sabate, R., and J. Estelrich. 2002. Aggregation characteristics of ovalbumin in β-sheet conformation determined by spectroscopy. Biopolymers 67:113-120.
[27] Haurowitz, F., F. Dimoia, and S. Tekman. 1952. The Reaction of Native and Denatured Ovalbumin with Congo Red. Journal of the American Chemical Society 74:2265-2271.
[28] Veerman, C., G. de Schiffart, L. M. C. Sagis, and E. van der Linden. 2003. Irreversible self-assembly of ovalbumin into fibrils and the resulting network rheology. Int J Biol Macromol 33:121-127.
[29] Kato, A., and T. Takagi. 1988. Formation of Intermolecular Beta-Sheet Structure during Heat Denaturation of Ovalbumin. J Agr Food Chem 36:1156-1159.
[30] Tanaka, N., Y. Morimoto, Y. Noguchi, T. Tada, T. Waku, S. Kunugi, T. Morii, Y. F. Lee, T. Konno, and N. Takahashi. 2011. The Mechanism of Fibril Formation of a Non-inhibitory Serpin Ovalbumin Revealed by the Identification of Amyloidogenic Core Regions. Journal of Biological Chemistry 286:5884-5894.
[31] Weijers, M., K. Broersen, P. A. Barneveld, M. A. C. Stuart, R. J. Hamer, H. J. De Jongh, and R. W. Visschers. 2008. Net Charge Affects Morphology and Visual Properties of Ovalbumin Aggregates. Biomacromolecules 9:3165-3172.
[32] Lara, C., S. Gourdin-Bertin, J. Adamcik, S. Bolisetty, and R. Mezzenga. 2012. Self-Assembly of Ovalbumin into Amyloid and Non-Amyloid Fibrils. Biomacromolecules 13:4213-4221.

[33] Sagis, L. M. C., C. Veerman, and E. van der Linden. 2004. Mesoscopic properties of semiflexible amyloid fibrils. Langmuir 20:924-927.
[34] Oosawa, F., & Kasai, M. (1962). A theory of linear and helical aggregations of macromolecules. Journal of molecular biology, 4(1):10-21.
[35] Cohen, S. I. A., M. Vendruscolo, C. M. Dobson, and T. P. J. Knowles. 2011. Nucleated polymerization with secondary pathways. III. Equilibrium behavior and oligomer populations. Journal of Chemical Physics 135.
[36] Sawaya, M. R., Sambashivan, S., Nelson, R., Ivanova, M. I., Sievers, S. A., Apostol, M. I., ... & Eisenberg, D. (2007). Atomic structures of amyloid cross-β spines reveal varied steric zippers. Nature, 447(7143), 453-457.
[37] Fitzpatrick A.W., D. G., Clare D.K., C. M., Wang L., L. V., Waudby C.A., M. H., Saibil H.R., V. M., & Griffin R.G., D. C. (2013). Atomic Structure and hierarchical assembly of a cross-β amyloid fibril. Proc. Nat. Acad. Sci. USA , 110 (4), 5468-5473.
[38] Kodali, R., and R. Wetzel. 2007. Polymorphism in the intermediates and products of amyloid assembly. Current Opinion in Structural Biology 17:48-57.
[39] Giehm, L., C. L. P. Oliveira, G. Christiansen, J. S. Pedersen, and D. E. Otzen. 2010. SDS-Induced Fibrillation of α-Synuclein: An Alternative Fibrillation Pathway. Journal of Molecular Biology 401:115-133.
[40] Necula, M., C. N. Chirita, and J. Kuret. 2003. Rapid anionic micelle-mediated α-synuclein fibrillization in vitro. Journal of Biological Chemistry 278:46674-46680.
[41] Hatters, D. M., C. E. MacPhee, L. J. Lawrence, W. H. Sawyer, and G. J. Howlett. 2000. Human apolipoprotein C-II forms twisted amyloid ribbons and closed loops. Biochemistry 39:8276- 8283.
[42] Xue, W. F., A. L. Hellewell, W. S. Gosal, S. W. Homans, E. W. Hewitt, and S. E. Radford. 2009. Fibril Fragmentation Enhances Amyloid Cytotoxicity. Journal of Biological Chemistry 284:34272-34282.